Basis for viscoelastic modelling of polyethylene terephthalate (PET) near Tg with parameter identification from multi-axial elongation experiments

Yun Mei Luo · Luc Chevalier · Eric Monteiro

Abstract The mechanical response of Polyethylene Terephthalate (PET) in elongation is strongly dependent on temperature, strain and strain rate. Near the glass transition temperature T_g, the stress vs strain curves present a strain hardening effect vs strain under conditions of large deformations. At a given strain value, the strain rate has also an increasing influence on the stress value. The main goal of this work is to propose a visco-elastic model to predict the PET behaviour when subjected to large deformations and to determine the material properties from the experimental data. The visco-elastic model is written in a Leonov like way and the variational formulation is carried out for the numerical simulation using this model. To represent the non–linear effects, an elastic part depending on the elastic equivalent strain and a non-Newtonian viscous part depending on both viscous equivalent strain rate and cumulated viscous strain are tested. The model parameters can then be accurately obtained through the comparison with the experimental uniaxial and biaxial tests.

Keywords Identification · Visco-elastic · Nonlinear behaviour · Experimental uniaxial and biaxial tests · Numerical simulation

Introduction

Polyethylene terephthalate (PET) under conditions of large deformations, during high strain rate elongation at temperature near the glass transition Tg, exhibits a pronounced nonlinear behaviour where non linear viscous and elastic effects appear. Both hyperelastic [1, 2] and viscoplastic [3] approaches cannot represent accurately this behaviour. In addition, classical visco-elastic models such as the Upper Convected Maxwell (UCM) model [4] or the Giesekus model do not adequately demonstrate this reaction. Chevalier and Marco [5] have performed biaxial tension tests near Tg with a range of strain rates from 0.02 s^{-1} to 2 s^{-1}. As illustrated in Fig. 1, a significant strain hardening effect was observed for the PET behaviour during these tension tests. Furthermore, they also carried out the relaxation tests [6]. The parameters like the relaxation time have been identified from these tests and clearly demonstrate the contribution of a viscous part in a highly elastic macromolecular network. The influence of temperature and strain rate on the relaxation time was mentioned: for a given strain rate, the relaxation time increases with the temperature; for a given temperature, the relaxation time increases when the strain rate decreases.

Therefore, a visco-elastic behaviour should reproduce more accurately the experimental responses.

In the first section of this paper, inspired by Figiel and Buckley [7], the assumption of an additive decomposition of elastic and viscous strain rate tensors ($\underline{\underline{D}} = \underline{\underline{D_e}} + \underline{\underline{D_v}}$) was adopted to describe the kinematic structure of the constitutive models. This choice, together with the assumption of zero viscous spin and the Oldroyd derivation of the elastic left Cauchy-Green tensor $\underline{\underline{B_e}}$, lead to a differential equation of the $\underline{\underline{B_e}}$ which is more stable than UCM or Giesekus model during the numerical simulation. The form of this equation is similar to the Leonov equation which is a differential equation of the elastic Finger tensor and the irreversible strain rate tensor (see [8] and Appendix A for details).

The numerical implementation is then presented and compared with analytical solution of uniaxial and biaxial

Y. M. Luo (✉) · L. Chevalier · E. Monteiro
Université Paris-Est, Laboratoire Modélisation et Simulation Multi Echelle, MSME UMR 8208 CNRS, 5 bd Descartes, 77454 Marne-la-Vallée, France
e-mail: yunmei.luo@univ-paris-est.fr

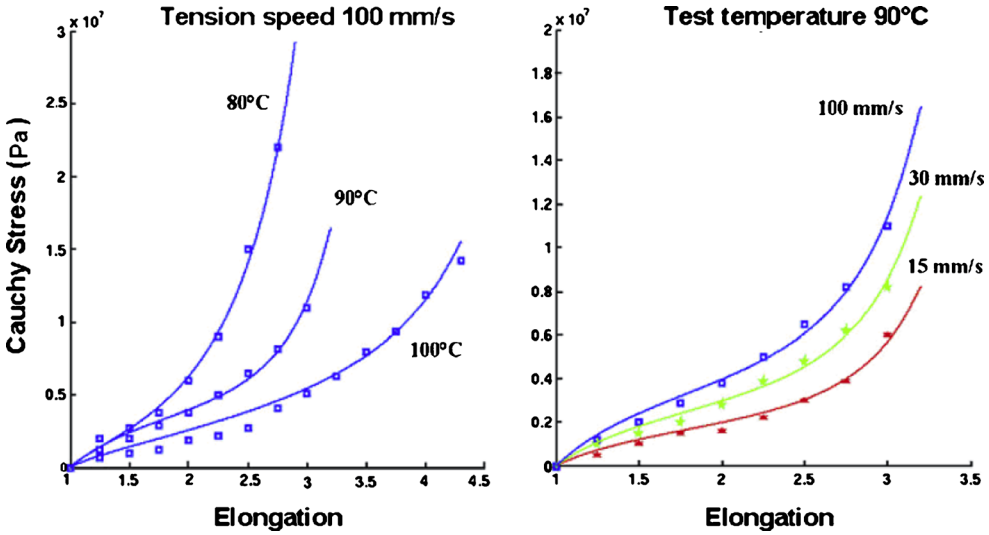

Fig. 1 Equi-biaxial tension test results. Initial shape of the specimen is square (50 mm side length) [5]

elongation in the linear case (i.e. constant values of shear modulus G and viscosity η). The modelling for uniaxial and biaxial elongations does not highlight any singularity, but it does not show the strain hardening effect which occurs in the experimental results.

Recently, experimental uniaxial and biaxial tests performed on PET were carried out by Menary et al. [9] in Queen's University of Belfast. These tension tests were performed with various tension speeds (from 1 s^{-1} to 32 s^{-1}) and various temperatures. Here we focus on the influence of the strain rate and we consider only the tests performed at temperature 90 °C. In order to represent the PET behaviour during the tests, the nonlinear forms of elastic and viscous characteristics $G(\varepsilon_e)$ and $\eta(\dot{\varepsilon}_v, \varepsilon_v)$ are proposed. The model parameters can be finally identified through the comparison with the experimental uniaxial and biaxial tests.

An incompressible large strain visco-elastic model

Figiel and Buckley [7] have suggested building a visco-elastic model adapted to highly elastic polymers as an extension of the hyper elastic approach used for rubber like materials coupled with a viscous part. In their proposition the viscous part has been supposed to be incompressible, the volume variation under pressure has been assumed to be purely elastic. In the following, considering the difficulty to provide data to identify the volume variation, we differ slightly considering both parts as incompressible. In the linear case, both relations can be written:

$$\begin{aligned} \underline{\sigma} &= 2G\underline{\underline{\varepsilon_e}} - p_e\underline{I} \\ \underline{\sigma} &= 2\eta\underline{\underline{D_v}} - p_v\underline{I} \end{aligned} \tag{1}$$

$\underline{\sigma}$ is the Cauchy stress tensor, $\underline{\underline{D_v}}$ is the symmetric part of the viscous velocity gradient and the double underscore means it is a second order tensor. $\underline{\underline{\varepsilon_e}}$ is the elastic part of the Eulerian strain measure defined by:

$$\underline{\underline{\varepsilon_e}} = \frac{1}{2}\left(\underline{\underline{B_e}} - \underline{I}\right) \tag{2}$$

where $\underline{\underline{B_e}}$ is the elastic part of the left Cauchy-Green tensor. p_e and p_v are pressures associated with the incompressible conditions of both parts:

$$\det \underline{\underline{B_e}} = 1, \qquad div\,\vec{V}_v = trace\underline{\underline{D_v}} = 0 \tag{3}$$

where $\vec{V}_v$ is the viscous velocity.

The assumption of an additive decomposition of the elastic and viscous strain rate tensors (respectively $\underline{\underline{D_e}}$ and $\underline{\underline{D_v}}$) is adopted to describe the kinematic structure of this model:

$$\underline{\underline{D}} = \underline{\underline{D_e}} + \underline{\underline{D_v}} \tag{4}$$

Combining Eq. 1 and the elastic and viscous strain rates in the Oldroyd derivation of the elastic left Cauchy-Green tensor, one can obtain the Leonov like Eq. 5 (see Appendix A for details):

$$\frac{\delta\underline{\underline{B_e}}}{\delta t} + \frac{1}{\theta}\underline{\underline{B_e}}.\underline{\underline{\widehat{B_e}}} = 0 \tag{5}$$

where θ is the relaxation time, ratio of the viscosity η and elastic shear modulus G. The subscript "^" denotes the deviatoric part of the tensor. The Oldroyd derivation $\delta\underline{\underline{B_e}}/\delta t$ is defined by:

$$\frac{\delta\underline{\underline{B_e}}}{\delta t} = \underline{\underline{\dot{B}_e}} + \underline{\underline{B_e}}\,\underline{\underline{\Omega}} - \underline{\underline{\Omega}}\,\underline{\underline{B_e}} - a\left(\underline{\underline{B_e}}\,\underline{\underline{D}} + \underline{\underline{D}}\,\underline{\underline{B_e}}\right) \text{ with a} = 1. \tag{6}$$

where is $\underline{\underline{\Omega}}$ the global spin.

Variational formulation for numerical simulation

Using the Eqs. 1, 2, 3, 4 and 5, the weak form of the problem leads to a 4 field formulation (velocity $\underline{V}$, the elastic left Cauchy Green tensor $\underline{\underline{B_e}}$ and the pressures p_e and p_v related to the incompressibility assumptions respectively for the elastic and the viscous parts). The matrix form degenerates because more than one third of the entries on its diagonal are zeros. In order to solve this ill-conditioned problem, we used a Zener like model by adding a Newtonian branch in parallel as shown schematically on Fig. 2.

We chose a small value of the viscosity η_N in the Newtonian branch (negligible in regard of η), so the behaviour law in Eq. 1 can be written:

$$\begin{aligned}\underline{\underline{\sigma}} &= \left(2\eta_n\underline{\underline{D}} - p\underline{\underline{I}}\right) + \left(2G\underline{\underline{\varepsilon_e}} - p_e\underline{\underline{I}}\right)\\ \underline{\underline{\sigma}} &= \left(2\eta_n\underline{\underline{D}} - p\underline{\underline{I}}\right) + \left(2\eta\underline{\underline{D_v}} - p_v\underline{\underline{I}}\right)\end{aligned} \tag{7}$$

where p is the pressure associated with the incompressibility condition of the global part. Furthermore, we can write the Eq. 7 in the following way:

$$\underline{\underline{\sigma}} = 2\eta_n\underline{\underline{D}} + \underline{\underline{\widehat{\sigma}}} - p\underline{\underline{I}} - q\underline{\underline{I}}$$

with

$$\underline{\underline{\widehat{\sigma}}} = G\underline{\underline{\widehat{B}_e}} = 2\eta\underline{\underline{D_v}} \qquad \Rightarrow \underline{\underline{D_v}} = \frac{G}{2\eta}\underline{\underline{\widehat{B}_e}} \tag{8}$$

and

$$q = p_e + G - G\frac{trace(B_e)}{3} = p_v$$

We assumed that the body and gravitational forces can be neglected. In the plane stress cases of uni and equibiaxial elongations, considering the incompressibility, the pressure p is given by Eq. 9:

$$\sigma_{33} = 0 \Rightarrow p + q = -2\eta_N(D_{11} + D_{22}) + \frac{G}{3} \times \left(\frac{2}{B_{e11}B_{e22} - B_{e12}^2} - B_{e11} - B_{e22}\right) \tag{9}$$

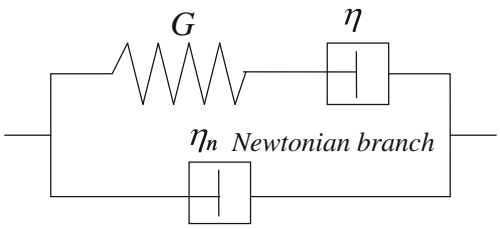

Fig. 2 Schematic representation of the proposed model. The visco-elastic branch is represented as a Maxwell model but the formulation is quite different. The Newtonian branch is placed in parallel for numerical reasons

The visco-elastic model is implemented in the Matlab environment using a finite element approach. A "2 fields" variational formulation (global velocity V and the elastic left Cauchy Green tensor B_e) is proposed for the plane stress incompressible problem. Some manipulations of Eqs. 5, 8 and 9 lead to the following weak form:

$$\begin{aligned}R_V = {} & 2\eta_N\int_\Omega \underline{\underline{D}}^* : \underline{\underline{D}}d\Omega + G\int_\Omega \underline{\underline{D}}^* : \underline{\underline{\widehat{B}_e}}d\Omega + 2\eta_N\int_\Omega \underline{\underline{D}}^* : \underline{\underline{I}}(D_{11} + D_{22})\\ & d\Omega - \frac{G}{3}\int_\Omega \underline{\underline{D}}^* : \underline{\underline{I}}\frac{1}{B_{e11}B_{e22} - {B_{e12}}^2}d\Omega - \int_{\partial\Omega_F}\underline{V}^*\underline{F}^d dS = 0;\end{aligned}$$

$$R_{B_e} = \int_\Omega \underline{\underline{B_e}}^* : \left(\frac{\delta\underline{\underline{B_e}}}{\delta t} + \frac{G}{\eta}\underline{\underline{B_e}}\,\underline{\underline{\widehat{B}_e}}\right)d\Omega = 0 \tag{10}$$

where the superscript * designates the virtual quantities (associated to the test functions in the finite element method) and F^d the prescribed traction field over the boundary $\partial\Omega_F$ where the loads are imposed. The integral equations are studied on the entire volume of the specimen Ω.

This strongly nonlinear problem (finite elastic displacements, elastic left Cauchy Green tensor $\underline{\underline{B_e}}$, with non constant shear modulus G and viscosity η), is solved using a classical Newton–Raphson iterative procedure (see Appendix B for details).

On the other hand in the cases of homogeneous and plane stress uniaxial and equibiaxial elongations, we can provide an analytical solution. The Cauchy stress tensor $\underline{\underline{\sigma}}$ and the strain rate tensor $\underline{\underline{D}}$, writes:

$$\begin{aligned}\underline{\underline{\sigma}} &= \begin{pmatrix}\sigma_U & 0 & 0\\ 0 & 0 & 0\\ 0 & 0 & 0\end{pmatrix} \text{ and } \underline{\underline{\mathrm{D}}} = \begin{pmatrix}\dot{\varepsilon} & 0 & 0\\ 0 & -\dot{\varepsilon}/2 & 0\\ 0 & 0 & -\dot{\varepsilon}/2\end{pmatrix};\\ \underline{\underline{\sigma}} &= \begin{pmatrix}\sigma_B & 0 & 0\\ 0 & \sigma_B & 0\\ 0 & 0 & 0\end{pmatrix} \text{ and } \underline{\underline{\mathrm{D}}} = \begin{pmatrix}\dot{\varepsilon} & 0 & 0\\ 0 & \dot{\varepsilon} & 0\\ 0 & 0 & -2\dot{\varepsilon}\end{pmatrix}\end{aligned} \tag{11}$$

One can solve Eq. 5 and then, substituting in Eq. 8, can obtain the elongation uniaxial and biaxial stresses, respectively σ_U and σ_B versus time or global elongation. For uniaxial and biaxial elongations, the related elastic elongations λ_e are given from the differential relations:

$$\dot{\lambda}_e/\lambda_e + \left(\lambda_e^2 - 1/\lambda_e\right)/3\theta = \dot{\varepsilon};\ \dot{\lambda}_e/\lambda_e + \left(\lambda e^2 - 1/\lambda_e^4\right)/6\theta = \dot{\varepsilon} \tag{12}$$

where $\dot{\varepsilon}$ is the global strain rate. The related stresses are then:

$$\begin{aligned}\sigma_U &= 3\eta_N\dot{\varepsilon} + G\left(\lambda_e^2 - 1/\lambda_e\right)\\ \sigma_B &= 6\eta_N\dot{\varepsilon} + G\left(\lambda_e^2 - 1/\lambda_e^4\right)\end{aligned} \tag{13}$$

From Table 1, one can evaluate the relaxation time θ=5 s. Uni and biaxial elongations at constant extension rate $\dot{\varepsilon}$ are considered. Figure 3 shows the results of the analytical approach (see Eq. 13) and numerical simulation (Eq. 10 solved using finite elements) are equal, for both elongation cases (uniaxial and biaxial) at a strain rate 8 s^{-1}. Furthermore, it shows that the stress–strain curves for PET are strongly dependent on the strain rate. As strain rate increases, the whole stress level is found to increase. Even if the modelling for uniaxial and biaxial elongations does not highlight any singularity, the comparison with experimental results of similar tests performed on PET at a temperature slightly over T_g, is not satisfactory. First, the experimental data presents a strain hardening effect (stress increases); second, double the strain rate does not double the asymptotic stress (viscosity presents a softening effect with strain rate); last, at the same value of the elongation λ, biaxial stress is not twice the uniaxial stress. For all these reasons, a non linear version of this model is necessary and discussed in the following.

Towards non-linear visco-elastic modelling

Beyond the linear case, the structure of the visco-elastic model allows to test all non linear behaviour of the form:

$$\begin{aligned} \underline{\underline{\sigma}} &= 2G_0 f(\overline{\varepsilon_e})\underline{\underline{\varepsilon_e}} - p_e\underline{\underline{I}} \\ \underline{\underline{\sigma}} &= 2\eta_0 g\left(\dot{\overline{\varepsilon_v}}, \overline{\varepsilon_v}\right)\underline{\underline{D_v}} - p_v\underline{\underline{I}} \end{aligned} \tag{14}$$

where $\overline{\varepsilon_e}$ is the equivalent elastic strain, $\dot{\overline{\varepsilon_v}}$ is the equivalent viscous strain rate and $\overline{\varepsilon_v}$ is the equivalent viscous strain. In order to model the strain hardening effect, first, a hyperelastic model is chosen for the elastic part. This choice is often done by authors dealing with the strain hardening modelling. The Yeoh model [2], for example, can be used but the results of simulations show that, associated with the viscous part, using the non-linear elastic part does not lead to a strain hardening effect. This is understandable since the global strain rate, which is the sum of an elastic strain rate and a viscous strain rate (Eq. 4) is constant: consequently if the viscous part only depends on the viscous strain rate, the strain in the viscous branch will reach a constant value. Under the same stress level, the elastic branch will stabilise at an elastic strain that will remain constant even if the hyperelastic shows an increasing evolution. A hyperelastic branch is not enough for the visco-elastic model to present a strain hardening effect. In this work, we assume that the elastic part is a constant and the strain hardening effect is influenced by the nonlinear viscous part: $f(\overline{\varepsilon_e}) = 1$, $G = G_0$.

One can first identify the initial shear modulus G_0: its value can be estimated from the initial slope of the global experimental strain–stress curves because there is no viscous strain at the very beginning of the test. Table 2 shows that G_0 does not vary much from one strain rate to another. The value of G is chosen as 8 MPa.

Consequently, we focus on the non-linear viscous part of the model chosen as in Cosson and Chevalier [3] that identified a non linear incompressible viscoplastic model, which represents macroscopically the strain hardening effect observed during tension for high strain. We chose the same form of the viscous model:

$$\eta = \eta_0 h(\overline{\varepsilon_v}).\ \left(\frac{\dot{\overline{\varepsilon_v}}}{\dot{\varepsilon}_{ref}}\right)^{m-1} \tag{15}$$

The hardening effect is related to the h function which increases continuously with $\overline{\varepsilon}_v$ that can be obtained by comparison with the experimental tests.

Menary et al. [9] recently provided experimental tests at different strain rates for TF9 grade PET under equibiaxial deformation at temperature 90 °C. In order to identify the h function, we proposed the following way:

- For each strain rate, the stress–strain curve of the equibiaxial test, the evolution of the related elastic elongations λ_e can be obtain from Eq. 13:

$$\begin{aligned} &\sigma_B \approx G\left(\lambda_e^2 - 1/\lambda_e^4\right) \Rightarrow {\lambda_e}^6 - {\lambda_e}^4\left(\frac{\sigma_B}{G}\right) - 1 = 0 \\ &\Rightarrow {\lambda_e}^2 = \frac{S}{3} + \frac{1}{6}\left(108 + 8S^3 + 12\sqrt{81 + 12S^3}\right)^{1/3} \\ &\quad + \frac{2S^2}{3\left(108 + 8S^3 + 12\sqrt{81 + 12S^3}\right)^{1/3}} \end{aligned} \tag{16}$$

where: $S=\sigma_B/G$.

- Then, for each strain rate and for different value of the exponent m, the $\eta_0 h$ function can be computed from the equation following:

$$\eta_0 h(\overline{\varepsilon_v}) = \frac{G}{6}\frac{\left(\lambda_e^2 - 1/\lambda_e^4\right)}{\left(\frac{\dot{\overline{\varepsilon_v}}}{\dot{\varepsilon}_{ref}}\right)^{m-1} D_v} \tag{17}$$

where $\dot{\varepsilon}_{ref}$ is a reference strain rate that can be taken equal to 1 s^{-1} for sake of simplicity. $D_v = \dot{\varepsilon} - \dot{\lambda}_e/\lambda_e$ in the case of

Table 1 Material parameters used for the numerical and analytical comparison are taken from [7]

Property	Value
Viscosity η	16.5 MPa.s
Viscosity η_N	200 Pa.s
Shear modulus G	3.29 MPa

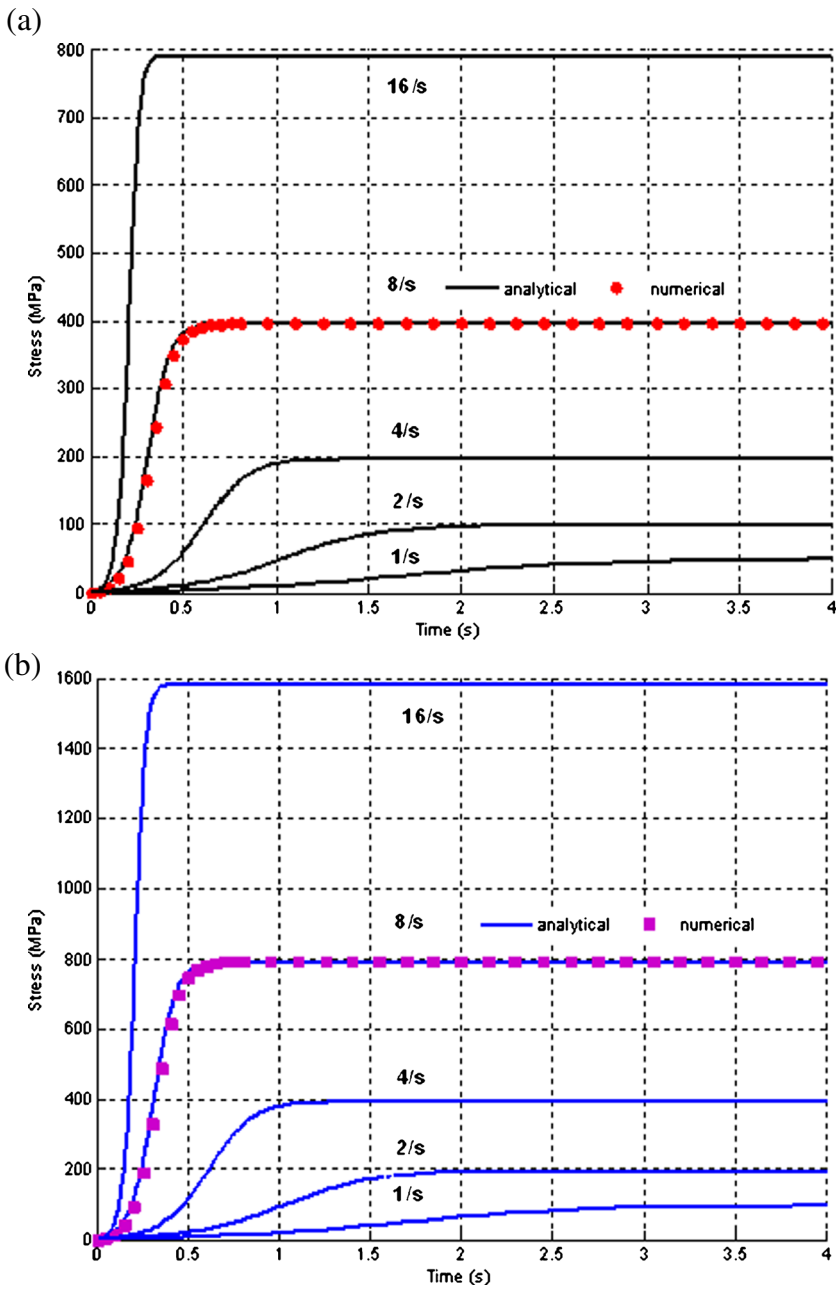

Fig. 3 Uniaxial (**a**) and biaxial (**b**) responses of the linear form of the visco-elastic model; Analytical results VS numerical results at a strain rate 8 s^{-1}

equibiaxial test. Equation 17 gives the $\eta_0 h$ evolution versus the equivalent viscous strain $\overline{\varepsilon}_v$ for each strain rate condition. The equibiaxial tests have been carried out for five global strain rates (1 s^{-1}, 2 s^{-1}, 4 s^{-1}, 8 s^{-1}, 16 s^{-1}).

Table 2 The numerical value of G_0

Strain Rate(/s)	1	2	4	8	16
G_0 (MPa)	7.2	8.1	7.7	7.9	8.9
Min G_0 (MPa)	7.2				
Max G_0 (MPa)			8.9		

– Each tension speed gives a different function $\eta_0 h$ versus $\overline{\varepsilon}_v$ for each value of exponent m. When we fixed the parameter m, we can sum the differences between each $\eta_0 h$ curve from each strain rate. The minimal dispersion is obtained for m equal to 0.25 as shown in Fig. 4.

Figure 4(a) illustrates the influence of the parameter m on the dispersion between the $\eta_0 h$ functions. With the optimal value of m, we obtained a similar evolution for the 5 curves of $\eta_0 h$ for each strain rate as shown in Fig. 4(b).

– We obtained a master curve for $\eta_0 h$ which highlights an asymptotic value for the equivalent viscous strain $\overline{\varepsilon}_v$ at about 2.1. This leads to an important increase of the

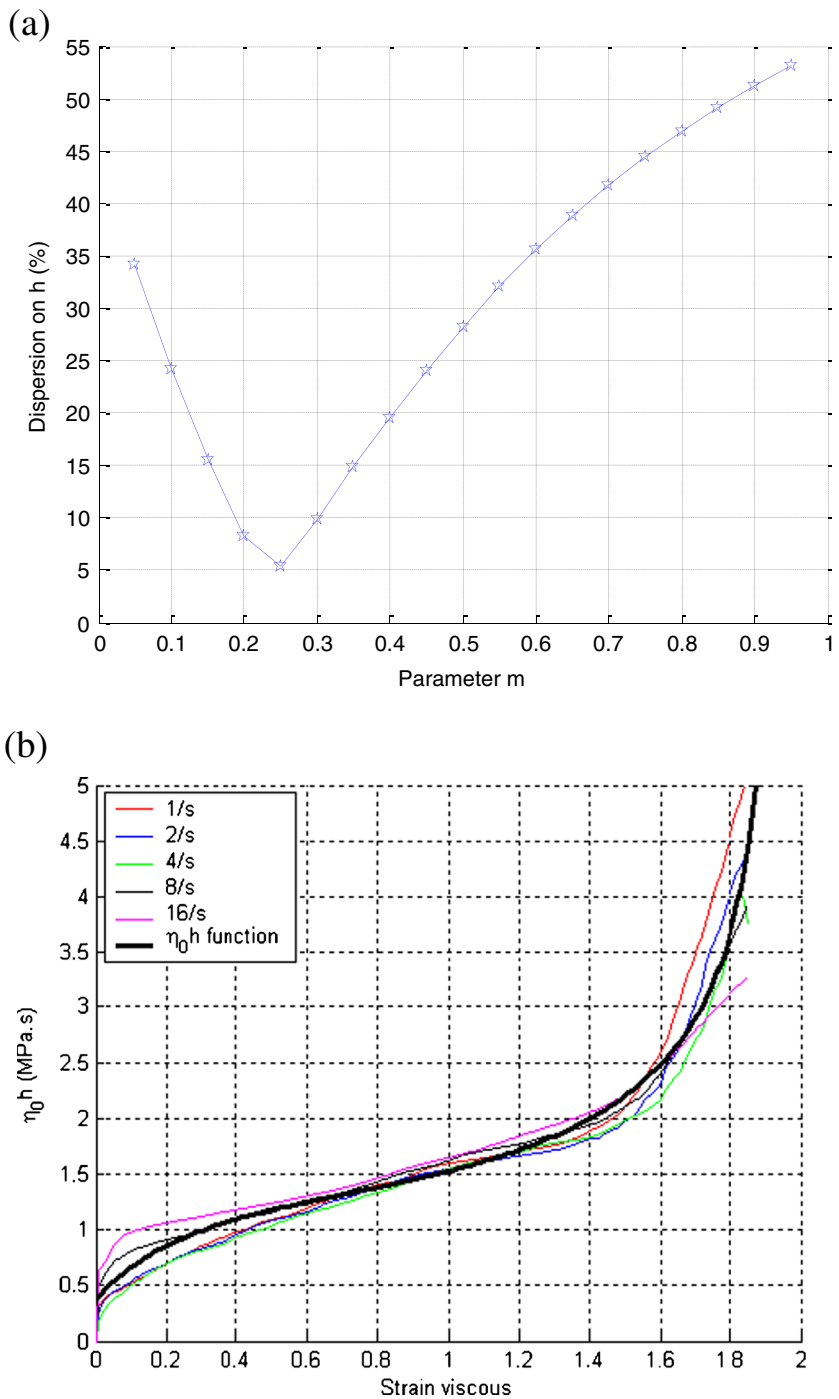

Fig. 4 **a** Minimization of differences between $h(\overline{\varepsilon}_v)$ function. An optimal value is obtained for m=0.25; **b** The $\eta_0 h$ evolution versus the equivalent viscous strain $\overline{\varepsilon}_v$ when m=0.25 and the $\eta_0 h$ function from Eq. 18

viscosity and a zero viscous strain rate when strain reaches this asymptotic value.

– The last step of the identification is to propose a model to represent the curve of the function h shown in Fig. 4(b). We can choose the $\eta_0 h$ function which varies exponentially with the viscous strain ε_v:

$$\eta_0 h(\overline{\varepsilon_v}) = \exp\left(a\overline{\varepsilon_v}^3 + b\overline{\varepsilon_v}^2 + c\overline{\varepsilon_v} + d\right) \tag{18}$$

With the exponential model, even if the steep part of the curve is not perfectly represented, a good representation of the $\eta_0 h$ data can be obtained (Fig. 4). Therefore, the characteristics of the PET for this model are:

$$m = 0.25, a = 7.355, b = -10.958, c = 5.168, d = -3.727.$$

It is clearly a phenomenological modelling where viscosity functions and shear elastic modulus evolution have no physical interpretation but we choose to limit our model to an additive composition of a spring and a dashpot for two reasons: (i) to limit the number of parameters and the complexity

of the model (ii) to propose an identification method easy to implement from uniaxial or biaxial tension tests.

In the following, we implemented this set of parameters into the stress–strain curve. Figure 5 shows that using the visco-elastic model with a non linear viscous part, we can obtain a substantially good representation of the strain hardening effect for different strain rates. The main difference between experimental data and the modelled biaxial

Table 3 Errors between the experimental and the results of the model

Strain Rate (/s)	Absolute Error (%)
1	8.8
2	9.9
4	8.4
8	7.1
16	12.8

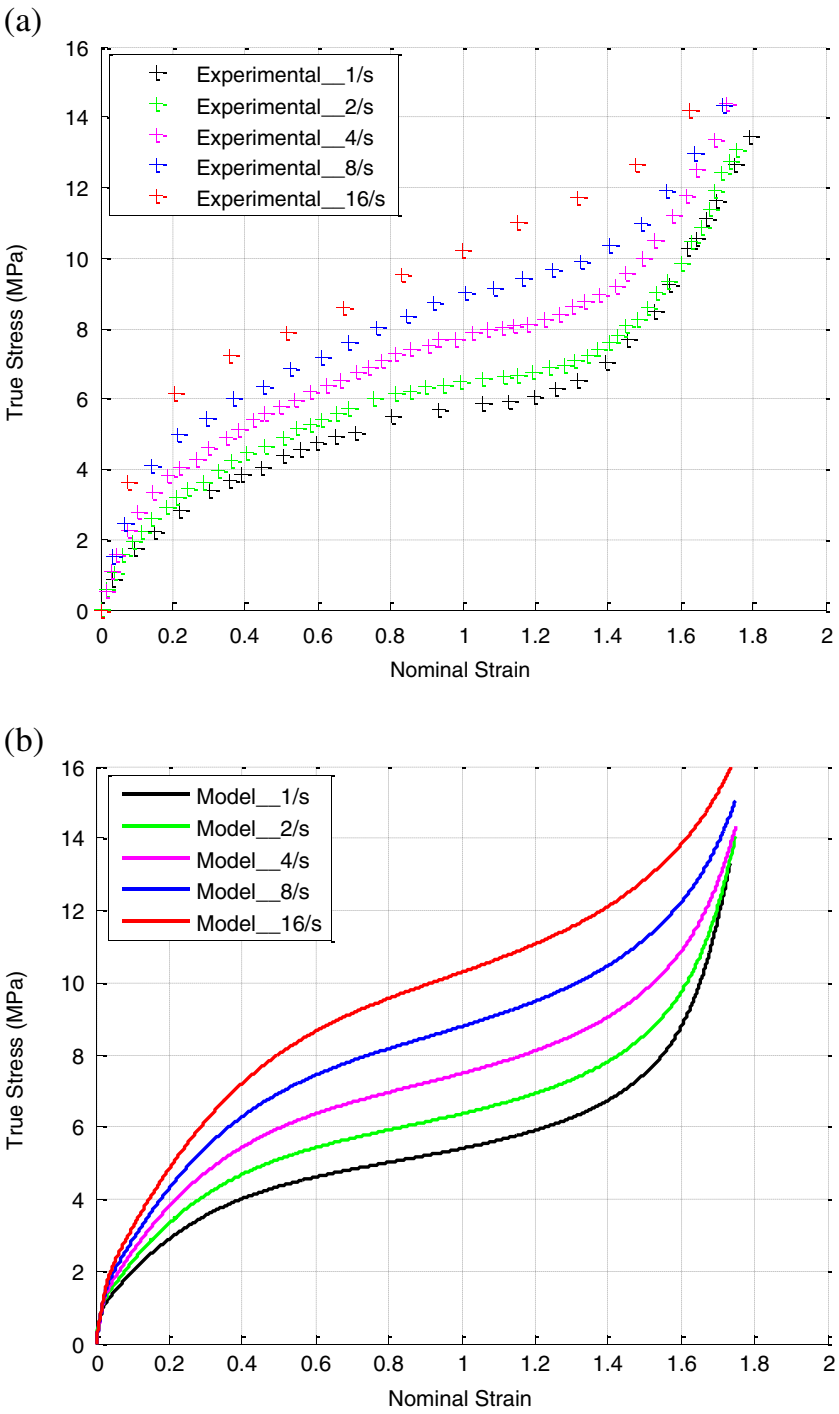

Fig. 5 **a** The data experimental [9]; **b** The results of the visco-elastic model

behaviour is the beginning of the stress–strain curve (when the strain is lower than 0.3): the experimental data initial slope seems to increase when the strain rate rises. This is in contradiction with the results of the model.

The relative differences between the experimental data and the results of this model are shown in Table 3.

Menary et al. [9] have also provided results on biaxial elongation tests at several temperatures (90 °C, 95 °C, 100 °C, 105 °C, 110 °C). Here we focus on a given strain rate: 8 s^{-1}. The global stress decreases in the stress–strain curve when the temperature increases. Since the viscosity usually depends on temperature, we add a function of temperature *g(T)* on the viscous model to represent this dependence. Therefore, Eq. 15 can be rewritten in the following form:

$$\eta = \eta_0 g(T) h(\overline{\varepsilon_v}). \left(\frac{\dot{\overline{\varepsilon_v}}}{\dot{\varepsilon}_{ref}}\right)^{m-1} \tag{19}$$

To identify the influence of temperature, we chose Williams-Landel-Ferry (WLF) model [10] which has proved to be widely applicable and we identified the WLF parameters C_1 and C_2 from the experimental data.

$$\ln(a_T) = \frac{-C_1(T - T_{ref})}{C_2 + T - T_{ref}} \tag{20}$$

One selects the reference parameter T_{ref} as: T_{ref}=90 °C. It appears that the shift a_T depending on temperature allows an approximate superposition. In this case, the coefficient C_1 and C_2 are obtained by a least-square fit of Eq. 20: $C_1 = 2.71$, $C_2 = 37.64^o C$.

We have implemented this set of parameters in order to reproduce the stress–strain curve (Fig. 6). For high temperatures, the experimental results show a very small strain hardening effect which is overestimated by the model. It is because we choose only one function of temperature in the viscosity. But if a dependence on the temperature was chosen in the *h* function it could represent the influence of *T* on the asymptotic viscous strain. The representation of the experimental results could be more accurate.

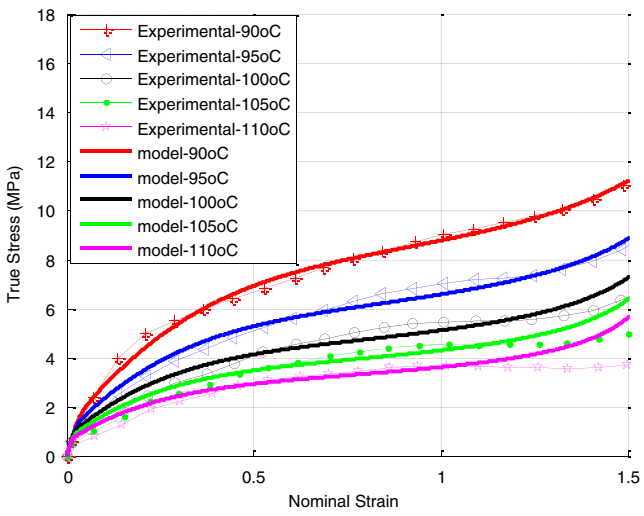

Fig. 6 The data experimental (the points) and the results of the viscoelastic model (the lines) at 8 s^{-1} under different temperatures (90 °C,95 °C,100 °C,105 °C,110 °C)

Conclusions

A basic visco-elastic model is proposed in the first part of the paper by introducing both an elastic part and a viscous part that lead to a Leonov like equation. Secondly, the weak form of the problem is achieved for the numerical simulation: simulations fit with analytical solution for uniaxial and biaxial tension tests. This visco-elastic model does not highlight singularities in the uniaxial or biaxial elongations for high strain rate and lead to a stable numerical scheme.

Considering the experimental results [5, 9], the behaviour of PET near T_g exhibits a strain hardening effect, that implies a non-linear viscous model to represent the viscous part of the behaviour behaviour. An identification procedure is proposed and leads to a good representation of the experimental data's of biaxial elongation tests.

In further work, we intend to simulate the stretch-blow moulding process together with an improvement of the behaviour law where the viscosity could be related to microscopic variables like crystallization ratio or shape factor of the microstructure. We can also model and identify accurately the temperature effect on PET behaviour. This model may be implemented to simulate using finite elements, the stretch blow moulding process for example.

Appendix A: Leonov like equation

The Oldroyd derivative of the elastic left Cauchy-Green tensor $\underline{\underline{B_e}}$ writes:

$$\frac{\delta \underline{\underline{B_e}}}{\delta t} = \dot{\underline{\underline{B_e}}} - \underline{\underline{L}}\,\underline{\underline{B_e}} - \underline{\underline{B_e}}\,\underline{\underline{L}}^T \tag{a}$$

where $\underline{\underline{L}}$ is the global velocity gradient. Considering the definition of $\underline{\underline{B_e}}$, the time derivative writes:

$$\dot{\underline{\underline{B_e}}} = \dot{\underline{\underline{F_e}}}\,\underline{\underline{F_e}}^T + \underline{\underline{F_e}}\,\dot{\underline{\underline{F}}}_e^T = \dot{\underline{\underline{F_e}}}\,\underline{\underline{F_e}}^{-1}\,\underline{\underline{F_e}}\,\underline{\underline{F_e}}^T + \underline{\underline{F_e}}\,\underline{\underline{F_e}}^T\,\underline{\underline{F_e}}^{-T}\,\dot{\underline{\underline{F}}}_e^T$$

$$\Rightarrow \dot{\underline{\underline{B_e}}} = \underline{\underline{L_e}}\,\underline{\underline{B_e}} + \underline{\underline{B_e}}\,\underline{\underline{L_e}}^T \tag{b}$$

where $\underline{\underline{L_e}}$ is the elastic velocity gradient. Substitution in Eq. (a) leads to:

$$\frac{\delta \underline{\underline{B_e}}}{\delta t} = \left(\underline{\underline{L_e}} - \underline{\underline{L}}\right)\underline{\underline{B_e}} + \underline{\underline{B_e}}\left(\underline{\underline{L_e}}^T - \underline{\underline{L}}^T\right) = \underline{\underline{L_v}}\,\underline{\underline{B_e}} + \underline{\underline{B_e}}\,\underline{\underline{L_v}}^T \tag{c}$$

where $\underline{\underline{L_v}}$ is the viscous velocity gradient. The approach used for dealing with the split between the elastic and viscous strains is the additivity of the elastic and viscous strain rates, but as explained in Figiel and Buckley [7] the spin partition does not make physical sense and one can assume that the spin is purely elastic. Consequently:

$$\underline{\underline{\Omega}} = \underline{\underline{\Omega_e}} \ , \underline{\underline{\Omega_v}} = \underline{\underline{0}} \quad \text{and} \underline{\underline{\mathrm{L_v}}} = \underline{\underline{\mathrm{D_v}}} \tag{d}$$

So Eq. (c) writes:

$$\frac{\delta \underline{\underline{B_e}}}{\delta t} = \underline{\underline{D_v B_e}} + \underline{\underline{B_e D_v}} \tag{e}$$

In the case of the linear behaviour laws, the deviatoric part of the Cauchy stress tensor can be expressed two different ways:

$$\left.\begin{array}{l} \underline{\underline{\widehat{\sigma}}} = 2G\underline{\underline{\widehat{\varepsilon}_e}} = G\underline{\underline{\widehat{B}_e} } \\ \underline{\underline{\widehat{\sigma}}} = 2\eta \underline{\underline{D_v}} \end{array}\right\} \Rightarrow \underline{\underline{D_v}} = \frac{G}{2\eta}\underline{\underline{\widehat{B}_e}} = \frac{1}{2\theta}\underline{\underline{\widehat{B}_e}} \tag{f}$$

where θ is the relaxation time, ratio of the viscosity η and elastic shear modulus G. It is easy to show that if the product between $\underline{\underline{D_v}}$ and $\underline{\underline{B_e}}$ does not necessary permute, the one between $\underline{\underline{B_e}}$ and $\underline{\underline{\widehat{B}_e}}$ does. So, combining Eqs. (e) and (f) leads to the Leonov like equation:

$$\frac{\delta \underline{\underline{B_e}}}{\delta t} + \frac{1}{\theta}\underline{\underline{B_e}}.\underline{\underline{\widehat{B}_e}} = 0 \tag{g}$$

Appendix B: Newton–Raphson iterative procedure

The nonlinear problem (finite elastic displacements, elastic left Cauchy Green tensor $\underline{\underline{B_e}}$, non constant shear modulus G and viscosity η), is solved using a classical Newton–Raphson iterative procedure. The consistent linearization must be done with Gâteaux operators and the linear form of the problem for the increment ΔV and ΔB_e is written in the following system:

$$\begin{bmatrix} [D_{\Delta V}\{R_V\}] & [D_{\Delta B_e}\{R_V\}] \\ [D_{\Delta V}\{R_{B_e}\}] & [D_{\Delta B_e}\{R_{B_e}\}] \end{bmatrix} \begin{Bmatrix} [\Delta V] \\ [\Delta B_e] \end{Bmatrix} = -\begin{Bmatrix} [R_V] \\ [R_{B_e}] \end{Bmatrix} \tag{i}$$

where $D_{\Delta V}\{R_V\}$, $D_{\Delta B_e}\{R_V\}$, $D_{\Delta V}\{R_{B_e}\}$ and $D_{\Delta B_e}\{R_{B_e}\}$ are the Gâteaux derivatives related to the increments:

$$D_{\Delta V}\{R_V\} = 2\eta_n \int_\Omega \underline{\underline{D}}^* : \underline{\underline{D(\Delta V)}} d\Omega + 2\eta_n \int_\Omega \underline{\underline{D}}^* : \left(\left(\underline{\underline{D(\Delta V)}} : \underline{\underline{I}} \right) \underline{\underline{I}} \right) d\Omega \tag{ii}$$

$$D_{\Delta B_e}\{R_V\} = \int_\Omega \underline{\underline{D}}^* : \left(G\Delta \underline{\underline{B_e}} \right) d\Omega - \int_\Omega \underline{\underline{D}}^* : \left(G \frac{1}{\Delta B_{e11}\Delta B_{e22} - \Delta B_{e12}{}^2} \underline{\underline{I}} \right) d\Omega$$

$$D_{\Delta V}\{R_{B_e}\} = 2\int_\Omega \underline{\underline{B_e}}^* : \left(\underline{\underline{B_e \Omega(\Delta V)}} \right) d\Omega - 2\int_\Omega \underline{\underline{B_e}}^* : \left(\underline{\underline{B_e D(\Delta V)}} \right) d\Omega$$

$$D_{\Delta B_e}\{R_{B_e}\} = \int_\Omega \underline{\underline{B_e}}^* : \Delta \underline{\underline{B_e}} d\Omega - 2\int_\Omega \underline{\underline{B_e}}^* : \left(\underline{\underline{\Omega}} \Delta \underline{\underline{B_e}} \right) d\Omega - 2\int_\Omega \underline{\underline{B_e}}^* : \left(\underline{\underline{D}} \Delta \underline{\underline{B_e}} \right) d\Omega + \int_\Omega \underline{\underline{B_e}}^* : \left(\frac{G}{\eta} \underline{\underline{B_e}} \Delta \underline{\underline{\hat{B}_e}} \right) d\Omega + \int_\Omega \underline{\underline{B_e}}^* : \left(\frac{G}{\eta} \underline{\underline{\hat{B}_e}} \Delta \underline{\underline{B_e}} \right) d\Omega$$

References

1. Marckmann G, Verron E, Peseux B (2001) Finite element analysis of blow molding and thermoforming using a dynamic explicit procedure. Polym Eng Sci 41(3):426–439
2. Yeoh OH (1993) Some forms of the strain energy function for rubber. Rubber Chemistry and technology 66(5):754–771
3. Cosson B, Chevalier L, Yvonnet J (2009) Optimization of the thickness of PET bottles during stretch blow molding by using a mesh-free (numerical) method. Int Polym Process 24(3):223–233
4. Schmidt FM, Agassant JF, Bellet M, Desoutter L (1996) Visco-elastic simulation of PET stretch/blow molding process. J Non-Newtonian Fluid Mech 64(1):19–42
5. Chevalier L, Marco Y (2006) Identification of a strain induced crystallization model for PET under Uni- and Bi-Axial loading: influence of temperature dispersion. Mech Mater 39:596–609
6. Chevalier L, Marco Y, Regnier G (2001) Modification des propriétés durant le soufflage des bouteilles plastiques en PET. Mec Ind 2:229–248
7. Figiel L, Buckley CP (2009) On the modeling of highly elastic flows of amorphous thermoplastic. Int J Non-linear Mech 44:389–395
8. Leonov AI (1976) Non equilibrium thermodynamics and rheology of visco-elastic polymer media. Rheologica Acta 15(2):85–98
9. Menary GH, Tan CW, Harkin-Jones EMA, Armstrong CG, Martin PJ () Biaxial deformation of PET at conditions applicable to the stretch blow molding process. Polymer Engineering & Science, in press
10. Williams ML, Landel RF, Ferry JD (1955) The temperature dependence of relaxation mechanisms in amorphous polymers and other glass-forming liquids. J Am Chem Soc 77 (14):3701–3707